Cell Reports

Article

Systemic Inflammation Suppresses Lymphoid Tissue Remodeling and B Cell Immunity during Concomitant Local Infection

Graphical Abstract

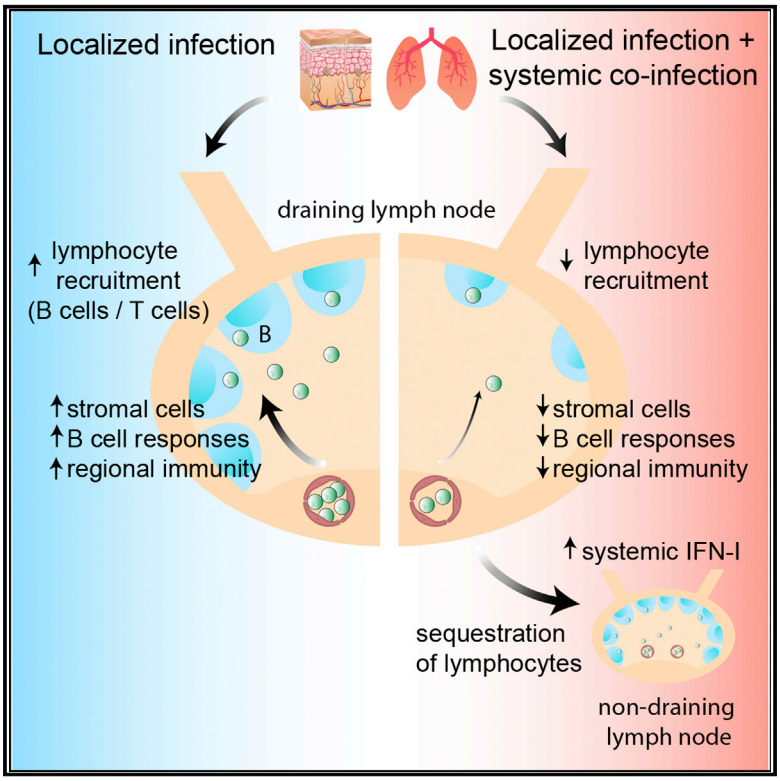

Highlights

- Systemic coinfection impairs the induction of immunity during local infection
- Systemic coinfection impairs stromal cell expansion in draining lymph nodes (dLN)
- Systemic coinfection suppresses B cell responses and antibody production
- Sequestration of lymphocytes in distal LN constrains immunity in dLNs

Authors

Yannick O. Alexandre, Sapna Devi, Simone L. Park, Laura K. Mackay, William R. Heath, Scott N. Mueller

Correspondence

smue@unimelb.edu.au

In Brief

Alexandre et al. reveal that systemic inflammation occurring concomitant with a localized infection or vaccination impairs the capacity to induce regional immunity. Inflammation-dependent lymphopenia impairs lymphocyte recruitment to draining lymph nodes and suppresses local tissue remodeling and B cell responses.

Alexandre et al., 2020, Cell Reports *33*, 108567
December 29, 2020
https://doi.org/10.1016/j.celrep.2020.108567

CellPress

Cell Reports

CellPress
OPEN ACCESS

Article

Systemic Inflammation Suppresses Lymphoid Tissue Remodeling and B Cell Immunity during Concomitant Local Infection

Yannick O. Alexandre,[1] Sapna Devi,[1,2] Simone L. Park,[1] Laura K. Mackay,[1,2] William R. Heath,[1,2] and Scott N. Mueller[1,2,3,*]
[1]Department of Microbiology and Immunology, The University of Melbourne, The Peter Doherty Institute for Infection and Immunity, Melbourne, VIC 3000, Australia
[2]The Australian Research Council Centre of Excellence in Advanced Molecular Imaging, The University of Melbourne, Melbourne, VIC 3000, Australia
[3]Lead Contact
*Correspondence: smue@unimelb.edu.au
https://doi.org/10.1016/j.celrep.2020.108567

SUMMARY

Concurrent infection with multiple pathogens occurs frequently in individuals and can result in exacerbated infections and altered immunity. However, the impact of such coinfections on immune responses remains poorly understood. Here, we reveal that systemic infection results in an inflammation-induced suppression of local immunity. During localized infection or vaccination in barrier tissues including the skin or respiratory tract, concurrent systemic infection induces a type I interferon-dependent lymphopenia that impairs lymphocyte recruitment to the draining lymph node (dLN) and induces sequestration of lymphocytes in non-draining LN. This contributes to suppressed fibroblastic reticular cell and endothelial cell expansion and dLN remodeling and impairs induction of B cell responses and antibody production. Our data suggest that contemporaneous systemic inflammation constrains the induction of regional immunity.

INTRODUCTION

Viral pathogens that infect the skin and mucosa, including herpes simplex virus (HSV) and influenza viruses, induce immune responses in lymph nodes (LNs) that drain the site of local infection. In contrast, many systemic pathogen infections including HIV, malaria, SARS-CoV-2, and bacterial sepsis, as well as other diseases including autoimmune disorders and stroke, result in systemic inflammation that can lead to immunosuppression by impacting different cellular components of the immune response. Multiple mechanisms have been shown to contribute to suppression of immune responses in response to viruses. Variants of lymphocytic choriomeningitis virus (LCMV) that cause chronic infections in mice (including LCMV clone 13) induce CD8 T cell-mediated destruction of antigen-presenting cells that contributes to suppression of antibody responses (Borrow et al., 1995; Odermatt et al., 1991). CD8 T cells can also contribute to immunosuppression by inducing the loss of antigen-specific B cells early during chronic LCMV infection (Fallet et al., 2016; Moseman et al., 2016). Moreover, people are often infected with multiple pathogens simultaneously, and such pathogen coinfections can impair immune responses and alter the outcomes of infections (Mabbott, 2018; Stelekati and Wherry, 2012). For instance, infection with LCMV can induce a CD8 T cell-mediated suppression of immunity against infection with vesicular stomatitis virus (VSV) administered weeks or months later (Leist et al., 1988; Roost et al., 1988). Although systemic infections or inflammatory responses are often correlated with reduced protection against localized coinfections (Chang et al., 2013; Edwards et al., 2015; Hotchkiss et al., 2013; Langhorne et al., 2000), the mechanisms underlying altered immunity during coinfection or inflammation remain poorly understood.

The induction of immune responses relies upon effective recruitment of B cells and T cells from the circulation where they can encounter cognate viral antigens presented by professional antigen presenting cells. Coordinated cellular interactions define T and B cell activation, proliferation, and differentiation, and these interactions are supported by specialized microanatomical compartments within LNs (Alexandre and Mueller, 2018). Networks of non-hematopoietic lymphoid stromal cells (LSCs) construct the microarchitecture of LNs, providing both structural and functional support for the induction of immune responses. Lymphatic endothelial cells (LECs) form the afferent and efferent lymphatic vessels required for sampling peripheral tissues and exit of lymphocytes back to the blood circulation, respectively. Lymphocytes that enter the LN from the blood are recruited via specialized blood endothelial cells (BECs) that form $PNAd^{+}$ high endothelial venules (HEVs) (Mueller and Germain, 2009). Subsets of mesenchymal fibroblastic reticular cells (FRCs) construct the LN architecture and include marginal reticular cells (MRCs), follicular dendritic cells (FDCs), T cell zone FRCs, and additional reticular cells localized in B cell follicles. FRCs are identified on the basis of expression of podoplanin (PDPN; also called gp38) and lack expression of the endothelial cell marker CD31. FRCs respond

dynamically to inflammation by modulating their gene expression program that influences immune responses (Gregory et al., 2017; Malhotra et al., 2012). This includes downregulation of the expression of the chemokines CCL19 and CCL21, which affects the positioning of CD8 and CD4 T cells (Mueller et al., 2007a). The importance of the mesenchymal LSC network was demonstrated in studies showing that depletion of the FRC network results in impaired induction of immune responses (Cremasco et al., 2014; Denton et al., 2014).

Localized infections induce considerable enlargement of the draining LNs to facilitate immune responses, including recruitment and proliferation of lymphocytes and expansion of stromal cell networks. T cell responses are initiated rapidly within LNs, with activation and proliferation of pathogen-specific T cells occurring in as little as 2 days, followed by egress of the expanded pool of effector cells after 5–6 days. B cell responses are initiated with similar rapidity, and B cells differentiate into short-lived antibody secreting cells (ASCs) within days, while other B cells migrate to B cell follicles to form germinal centers (GCs) and differentiate into high affinity plasma blasts (PBs) or memory B cells. GCs form within days after infection and can persist for weeks or months. LN expansion peaks 1–2 weeks after infection, which is delayed relative to the induction of T cell responses, suggesting that remodeling of LN stromal cell networks may be particularly important for supporting B cell responses. We have previously shown that LN remodeling after HSV infection requires recruitment of lymphocytes from the circulation to induce LN expansion, whereas B cells can sustain stromal cell responses (Gregory et al., 2017).

Here, we examined the impact of systemic infection on an ongoing local immune response. We show that the induction of systemic inflammation in response to coinfection of mice with LCMV or Toll-like receptor (TLR) agonists impaired LN swelling and stromal cell remodeling and inhibited B cell responses to localized infection or vaccination. Systemic inflammation induced a type I interferon (IFN-I)-dependent lymphopenia, impairing the recruitment of B cells to draining LNs and hindering the induction of humoral immune responses. Our findings reveal that a consequence of an acute systemic inflammatory response is the suppression of the ability to induce local immunity.

RESULTS

Restrained LN Remodeling and Suppressed B Cell Responses after LCMV Infection

We first investigated how different viral pathogens influence lymphoid tissue remodeling. We infected mice subcutaneously in the footpad with HSV or LCMV Armstrong and enumerated stromal cell populations in the draining popliteal LNs (pLNs) by flow cytometry 8 days after infection (Figure 1A). HSV inoculation results in an infection that remains localized to tissues near the site of inoculation (Gregory et al., 2017), whereas LCMV replicates locally as well as spreading systemically, including to the spleen (Jones et al., 2000; Olson et al., 2012). HSV infection induced a marked increase in total pLN cellularity and expanded all populations of pLN LSC: PDPN$^+$ FRC, PDPN$^+$ CD31$^+$ LEC, CD31$^+$ BEC, and CD31$^+$ PNAd$^+$ HEV (Figure 1B). In contrast, LCMV infection resulted in only a marginal increase in cellularity and no significant expansion of the subsets of LSCs in the LNs compared to uninfected mice (Figure 1B).

Examination of pLNs by confocal microscopy revealed substantial enlargement of the draining LNs after HSV infection, whereas pLNs were small and lacked organized B cell zones after LCMV infection (Figure 1C). Closer examination revealed substantial disorganization of the PDPN$^+$ T cell zone FRC network that ensheaths laminin$^+$ reticular fibers, with reduced PDPN-expressing cells covering the reticular network and disorganized reticular fibers (Figure 1D), as well as loss of B cell zone stromal cell organization after LCMV infection (Figure 1E). Notably, in LCMV-infected mice, B cell follicles were highly disorganized, and we could not detect FDC, whereas B cell follicle organization and FDCs were intact in HSV-infected mice (Figure 1E). Moreover, we observed the formation of a network of PDPN$^+$ FRCs on the capsular side of the B cell follicles in LCMV-infected mice (Figure 1E, yellow arrows). This indicated that the B cell follicles retracted from the LN capsule and a population of subcapsular PDPN$^+$ FRCs formed in this zone during LCMV infection.

Because MAdCAM-1$^+$ MRCs form a specialized stromal layer between B cell follicles and the subcapsular sinus, we postulated that the expanded subcapsular LSCs in LCMV-infected mice might be MRCs, but subsequent analysis revealed that MAdCAM-1$^+$ were not expanded following LCMV infection. Conversely, we observed a substantial increase in MAdCAM-1$^+$ PDPN$^+$ FRCs after HSV infection (Figure 1F). Greater than half of all FRC were MAdCAM-1$^+$ after HSV infection (Figure 1G), suggesting that expression of this adhesion molecule was upregulated after HSV but not LCMV infection. Staining of tissue sections confirmed increased expression of MAdCAM-1 on T cell zone FRCs in pLNs after HSV but not LCMV infection (Figure S1). This suggests that MAdCAM-1, which is typically used to define MRCs and is also expressed by FDCs in LNs, is not a reliable marker of MRCs after infection.

Next, we examined virus-specific CD8$^+$ T cell responses in the pLN by major histocompatibility complex class I (MHC-I) tetramer staining. Both local infection with LCMV and HSV infection induced robust numbers of virus-specific CD8$^+$ T cells (Figures 2A and 2B). In contrast, we found that B cell numbers were significantly reduced in draining pLN after LCMV infection in comparison with HSV-infected mice (Figure 2D). Expansion of GL7$^+$ GC B cells and CD138$^+$ ASCs was also significantly lower in the pLN after LCMV infection compared to HSV infection (Figures 2C–2E). B cell follicles were increased in size after HSV infection and contained GL7$^+$ GC B cells, while B cell follicles were markedly reduced in size, and GL7$^+$ cells were extrafollicular in LCMV-infected mice (Figure 2F). Large numbers of CD138$^+$ ASC accumulated at the border between T and B cell zones and within the medullary cords after HSV infection, whereas ASCs were reduced and only observed in the medulla during LCMV infection (Figure 2F). Thus, LCMV infection results in diminished LN remodeling, loss of B cell follicles, and restrained B cell responses in draining LNs.

LCMV Coinfection Suppresses LN Remodeling in Response to Localized Infection

The subdued stromal cell expansion and altered lymphoid tissue architecture observed following LCMV infection led us to

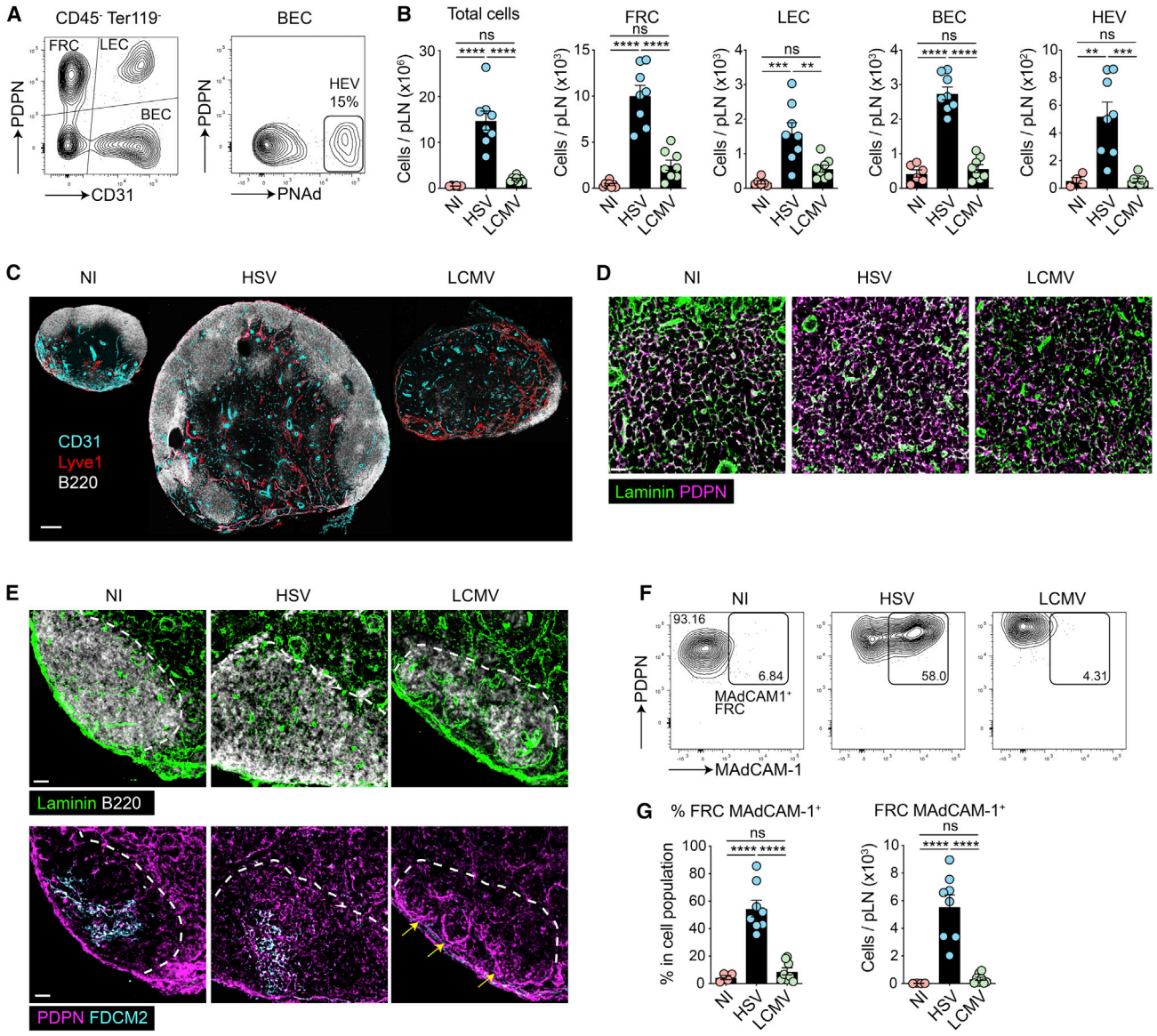

Figure 1. Restrained Remodeling of the Draining LNs during LCMV Infection

(A) Gating strategy to identify CD45$^-$ Ter119$^-$ stromal cell subsets by flow cytometry.

(B) Numbers of total cells and stromal cell subsets in the pLN from uninfected (NI) mice and mice infected subcutaneously (s.c.) with HSV or LCMV analyzed by flow cytometry on day 8. Graphs show pooled data (mean ± SEM) from 3 independent experiments each with 6–8 mice per group. *$p < 0.05$, **$p < 0.01$, ***$p < 0.001$, ****$p < 0.0001$, ns, non-significant, by ANOVA with Tukey's multiple comparisons test.

(C–E) pLN sections from NI-, HSV-, or LCMV-infected mice (d8) were stained for B220, Lyve1, and CD31 (C), laminin and podoplanin (D), or laminin, B220, podoplanin, and FDC-M2 (E) and analyzed by confocal microscopy. Data are representative of 2 experiments with 6 mice per group. Dotted lines depict border of B cell follicles and arrows show subcapsular FRCs in LCMV pLN that were not observed in NI or HSV pLN. Scale bars, 200 μm (C), 30 μm (D and E).

(F) MAdCAM-1 expression on FRC from NI mice and following HSV or LCMV infection.

(G) Percentage and numbers of MAdCAM-1$^+$ FRCs in the pLN of NI and mice infected s.c. with HSV or LCMV (day 8). Graphs show pooled data (mean ± SEM) from 3 independent experiments each with 6–8 mice per group. ****$p < 0.0001$, ns, non-significant, by ANOVA with Tukey's multiple comparisons test.

See also Figure S1.

investigate the impact of LCMV infection on LN remodeling during localized HSV coinfection. We infected mice with HSV in the footpad and coinfected the mice 2 days later with LCMV either by the same route or systemically by intraperitoneal infection (Figure 3A). LCMV coinfection by either route markedly restrained the increase in pLN cellularity induced by HSV infection and suppressed FRC expansion (Figure 3B). Local infection with LCMV resulted in infection of pLN FRCs whereas systemic LCMV infection did not (Figure S2A). Yet, both routes of infection resulted in equivalent suppression of the draining LN response

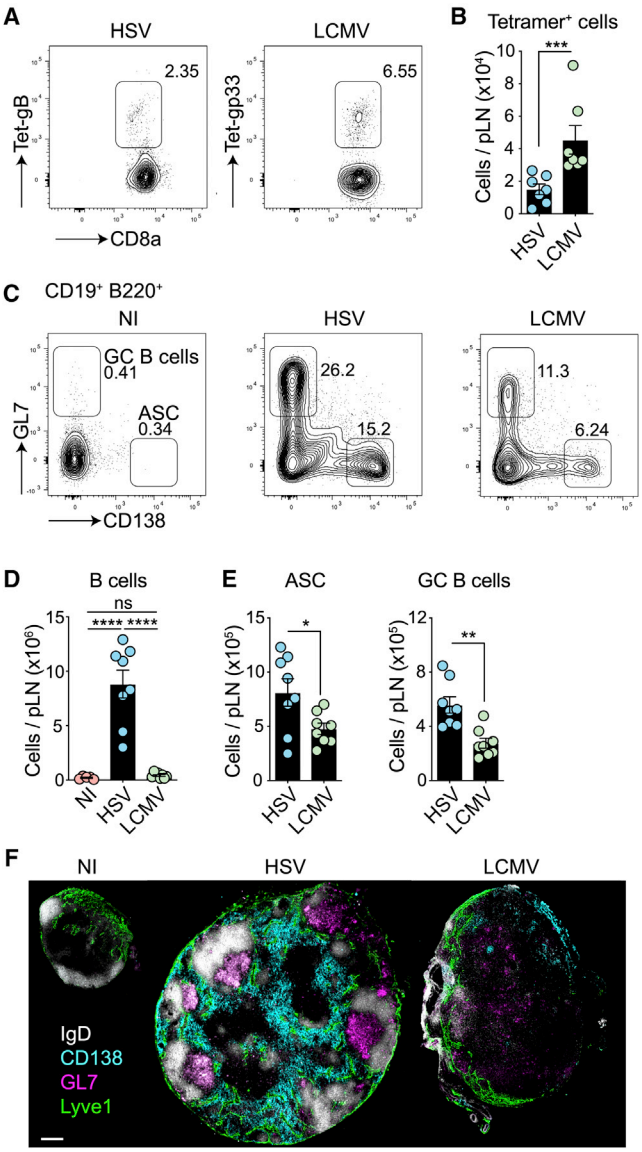

Figure 2. Suppressed B Cell Responses during LCMV Infection

(A) Tetramer staining of CD8$^+$ T cells, 8 days following s.c. HSV and LCMV infection.

(B) Numbers of CD8$^+$ Tetramer$^+$ cells in the pLN of HSV and LCMV-infected mice. Data are pooled from 2 independent experiments with 7 mice per group. ***$p < 0.001$, by Mann-Whitney test.

(C) Flow cytometry analysis of GL7$^+$ GC B cells and CD138$^+$ ASC. B cells were first gated on live CD19$^+$ CD3$^-$ NK1.1$^-$ cells.

(D) Absolute numbers of B cells in the popliteal LN from NI mice and mice infected s.c. with HSV or LCMV 8 days earlier. Graphs show pooled data (mean ± SEM) from 3 independent experiments each with 6–8 mice per group. ****$p < 0.0001$, ns, non-significant, by ANOVA with Tukey's multiple comparisons test.

(E) ASCs and GC B cells in the pLN from mice infected with HSV or LCMV. Graphs show pooled data (mean ± SEM) from 2 independent experiments with 8 mice per group. *$p < 0.05$, **$p < 0.01$, by unpaired two-tailed t test.

(F) pLN sections from NI-, HSV-, or LCMV-infected mice (d8) were stained for IgD, CD138, GL7, and Lyve1 and analyzed by confocal microscopy. Data are representative of 2 experiments with 6 mice per group. Scale bar, 200 μm.

(Figure 3B), ruling out an inhibitory role of LCMV through direct infection of FRCs. Because local LCMV infection also results in systemic spread of virus from the LN to spleen (Olson et al., 2012), we performed subsequent experiments using systemic LCMV coinfection. Importantly, LCMV coinfection did not alter the growth of HSV in the tissue (Figure 3C).

We examined HSV-draining pLN sections by confocal microscopy and discovered that LCMV coinfection prominently altered pLN remodeling in response to HSV. In coinfected mice, B cell follicles were small and disorganized, and LYVE-1$^+$ medullary sinuses were more prominent compared to mice infected with HSV alone (Figure 3D). Closer examination of B cell follicles in coinfected mice revealed fewer B cells, reduction of the FDC network within the follicles, and recession of the follicles away from the pLN subcapsular sinus (Figure 3E). Strikingly, a dense network of PDPN$^+$ FRC formed between B cell follicles and the pLN capsule in coinfected mice (Figure 3E, yellow arrows), similar to what we observed during local LCMV infection (Figure 1E), that was absent from mice infected with HSV alone.

Quantification of cells by flow cytometry revealed a significant reduction in total cellularity and reduced expansion of pLN FRCs, LECs, BECs, and PNAd$^+$ HEV in HSV-draining LNs from LCMV coinfected mice (Figure 3F). Coinfection suppressed the induction of MAdCAM-1 on FRCs (Figure 3G) resulting in a significant reduction in both MAdCAM-1$^+$ as well as MAdCAM-1$^-$ FRC (Figure S2B). We also examined CD157 (BP-3) expression on FRCs, a marker that has been used to identify subpopulations of FRCs including CD157-lo medullary FRCs (Huang et al., 2018). Both CD157$^+$ T cell zone FRCs and CD157-lo medullary FRC populations were reduced in the pLNs of mice coinfected with HSV and LCMV in comparison with mice infected with HSV alone (Figure 3H).

These data suggested that LCMV coinfection inhibited LN expansion in response to local HSV infection. To determine if systemic coinfection also suppressed dLN responses to other localized infections, we infected mice intranasally with influenza A virus X31 and coinfected these mice with LCMV 2 days later (Figure 3I). Coinfection suppressed immune responses in the draining mediastinal LNs (mLNs), resulting in reduced cellularity and impaired expansion of FRCs, LECs, BECs, and PNAd$^+$ HEV, as well as impaired upregulation of MAdCAM-1 by mLN FRCs compared to mice infected with influenza alone (Figure 3J). This indicated that systemic infection, concurrent with either a skin or respiratory viral infection, suppresses immune responses in the LN draining the site of localized challenge.

Because systemic coinfection suppressed expansion of pLN LSCs, we wanted to know if this was due to reduced proliferation or altered survival of LSC. We examined proliferating LSCs in LCMV and HSV coinfected mice by staining for Ki67. Significantly fewer Ki67$^+$ FRCs, LECs, and BECs were detected in coinfected mice when compared to mice infected with HSV alone (Figure 3K). A reduced proportion of LECs, BECs, and MAdCAM-1$^-$ FRCs expressed Ki67, indicating reduced proliferation of these cells (Figure 3L). In contrast, coinfection did not alter the number of apoptotic (annexin-V$^+$ PI$^+$) FRCs, LECs, or BECs compared to that observed following infection with HSV alone (Figure S2C). Further, we observed no alterations in metabolic functions as determined by glucose or lipid uptake,

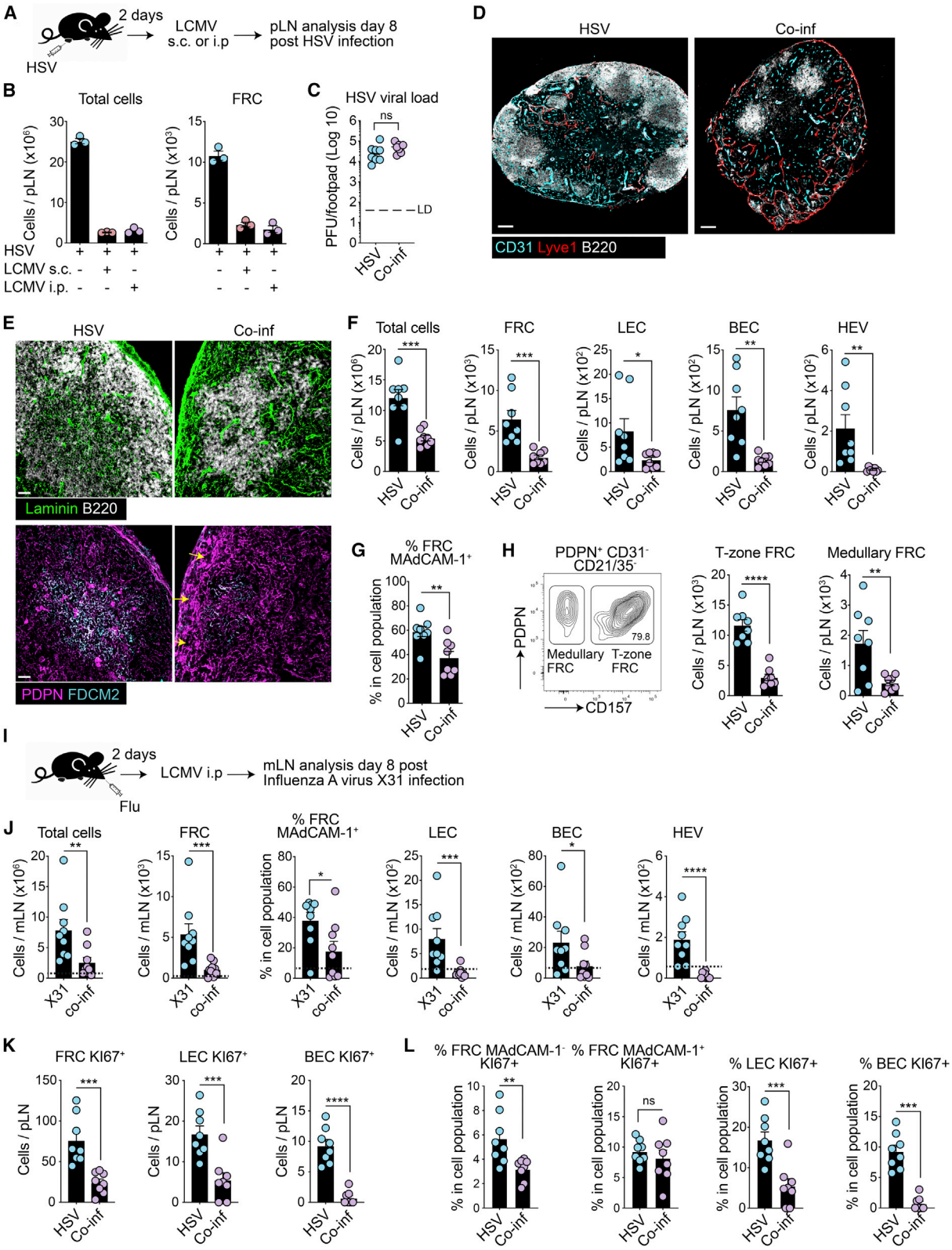

(legend on next page)

mitochondrial mass, or oxidative stress in pLN LSCs in coinfected mice compared to mice infected with HSV alone (Figures S2D and S2E). Thus, systemic LCMV coinfection suppressed dLN remodeling and stromal cell expansion in response to localized infection.

Systemic Coinfection Suppresses B Cell Responses to Localized Infection

We examined immune responses in HSV and LCMV coinfected mice and observed that although total numbers of $CD8^+$ T cells in the pLN were reduced by coinfection, HSV-specific $CD8^+$ T cell responses were unaffected (Figure 4A). Systemic LCMV coinfection also reduced the accumulation of total $CD4^+$ T cells in the draining pLN and suppressed the induction of T follicular helper (T_{FH}) cells compared to mice infected with HSV alone (Figures 4B and S3A). B cell numbers were significantly reduced in the pLN of coinfected mice, and the induction of GC B cells and ASCs was impaired (Figure 4C). This suppression of local B cell responses during LCMV coinfection was not due to increased apoptosis of polyclonal B cells or T cells, as indicated by annexinV staining (Figure 4D). Histological examination of pLN sections revealed a reduction in the number of $GL7^+$ GC and fewer $CD138^+$ plasma cells in coinfected mice (Figure 4E). Moreover, systemic LCMV coinfection significantly suppressed HSV-specific antibody responses (Figure 4F).

To further investigate the impact of systemic infection on the induction of local antigen-specific B cell responses, we examined ovalbumin (OVA)-specific B cell receptor transgenic OB-I B cell responses following transfer into B6 mice and immunization with OVA in complete Freund's adjuvant (OVA/CFA) (Figure 4G). OB-I B cells expanded significantly in the pLN following sub-cutaneous OVA/CFA immunization and formed GC B cells and ASCs (Figures 4H and S3B). Infection of mice with LCMV significantly impaired the expansion of the OB-I B cells in the pLN, reduced the number of GC cells and ASCs, and reduced the frequency of OB-I B cells that developed into GC cells and ASCs (Figures 4H and S3B). Together, these data show that systemic infection with an unrelated pathogen suppresses the induction of antigen-specific B cell responses in LN draining the site of a localized challenge.

Coinfection-Induced Lymphopenia Suppresses LN Expansion and B Cell Responses

CTL can kill virus-infected stromal cells and B cells during infection of mice with strains of LCMV that cause chronic infection (Moseman et al., 2016; Mueller et al., 2007b). To determine if $CD8^+$ T cells contributed to reduced LN expansion and B cell responses during coinfection with LCMV Armstrong, which is an acute infection, we infected mice with HSV then treated with depleting anti-CD8α antibody prior to LCMV coinfection (Figure 5A). Suppression of pLN remodeling and impairment of B cell responses in LCMV coinfected mice was unaffected by the loss of $CD8^+$ T cells (Figures 5B and S3C). Inflammatory monocytes can impair B cell responses during chronic LCMV infection (Sammicheli et al., 2016). However, B cell responses remained constrained during LCMV infection in $CCR2^{-/-}$ hosts with defective recruitment of monocytes (Figures S3D and S3E), suggesting that monocytes were not critical for suppression of the dLN response in this model.

The reduction in B and T lymphocytes in the pLN of LCMV coinfected mice led us to hypothesize that LCMV infection induces a general lymphopenia (Figure S5A) (Shiow et al., 2006) that traps lymphocytes in distal tissues and inhibits lymphocyte recruitment to the draining LN during peripheral viral infection. To examine this, we treated HSV-infected mice with the immunomodulatory drug FTY720 to induce a systemic lymphopenia (Halin et al., 2005) (Figure 5C). Expansion of pLN LSCs and upregulation of MAdCAM-1 by FRCs was impaired in FTY720-treated HSV-infected mice compared to untreated controls (Figure 5D). B cell accumulation, induction of GC B cells and ASCs (Figure 5E), and antibody responses (Figure 5F) were also inhibited in FTY720-treated mice, whereas virus-specific $CD8^+$ T cell responses were unchanged, suggesting that lymphopenia impairs the induction of local B cell responses and LN remodeling but not

Figure 3. LCMV Coinfection Suppresses Lymphadenopathy to Localized Infection

(A) Experimental schematic of coinfection. Mice were infected s.c. with HSV and 2 days later infected with LCMV s.c. or intraperitoneally (i.p.). pLNs were analyzed 8 days post HSV infection.

(B) Numbers of total cells and FRC in the pLNs of infected mice analyzed by flow cytometry. Graphs are representative of 2 experiments with 3 mice per group (mean ± SEM).

(C) HSV viral load in the footpad of infected mice. Mice were infected with HSV s.c. and LCMV i.p. (coinfection) and footpad tissue harvested 5 days post-HSV infection for plaque assay. Data are pooled from 2 independent experiments with 8 mice per group. ns, non-significant, by Mann-Whitney test. LD, limit of detection.

(D and E) pLN sections from NI, HSV or coinfected mice were stained for B220, Lyve1, and CD31 (D), Laminin, B220, podoplanin, and FDC-M2 (E), and analyzed by confocal microscopy. Data are representative of 2 experiments with 6 mice per group. Scale bar, 40 μm.

(F and G) Numbers of total cells and stromal cell subsets (F) and MAdCAM-1 expression analysis on FRCs (G) in the pLNs of HSV and coinfected mice analyzed by flow cytometry. Graphs show pooled data (mean ± SEM) from 2 independent experiments with 8 mice per group.

(H) Expression of CD157 on $PDPN^+$ $CD31^-$ CD21/35$^-$ cells to define T cell zone FRCs ($CD157^+$) and medullary FRCs ($CD157^-$) by flow cytometry. Graphs are pooled data of 2 experiments with 8 mice per group (mean ± SEM). *p < 0.05, **p < 0.01, ***p < 0.001, ****p < 0.0001, by unpaired two-tailed t test (F–H).

(I) Mice were infected intranasally with Flu-gB and 2 days later infected i.p. with LCMV. Mediastinal LNs (medLNs) were analyzed 8 days post flu infection.

(J) Numbers of total cells, stromal cell subsets, and MAdCAM-1 expression analysis on FRCs in the medLN of Flu and coinfected mice analyzed by flow cytometry. Graphs show pooled data (mean ± SEM) from 2 independent experiments with 8–9 mice per group. Baseline numbers of cells in uninfected LNs are indicated by dotted lines. *p < 0.05, **p < 0.01, ***p < 0.001, ****p < 0.0001, by Mann-Whitney test.

(K and L) Number (K) and proportion (L) of $Ki67^+$ stromal cell subsets following HSV and coinfection. Mice were infected as in (A) and pLN harvested 5 days post-HSV infection and intracellular KI67 expression was analyzed flow cytometry. Graphs show pooled data (mean ± SEM) from 2 independent experiments each with 8 mice per group. ***p < 0.001, ****p < 0.0001, by unpaired two-tailed t test.

See also Figure S2.

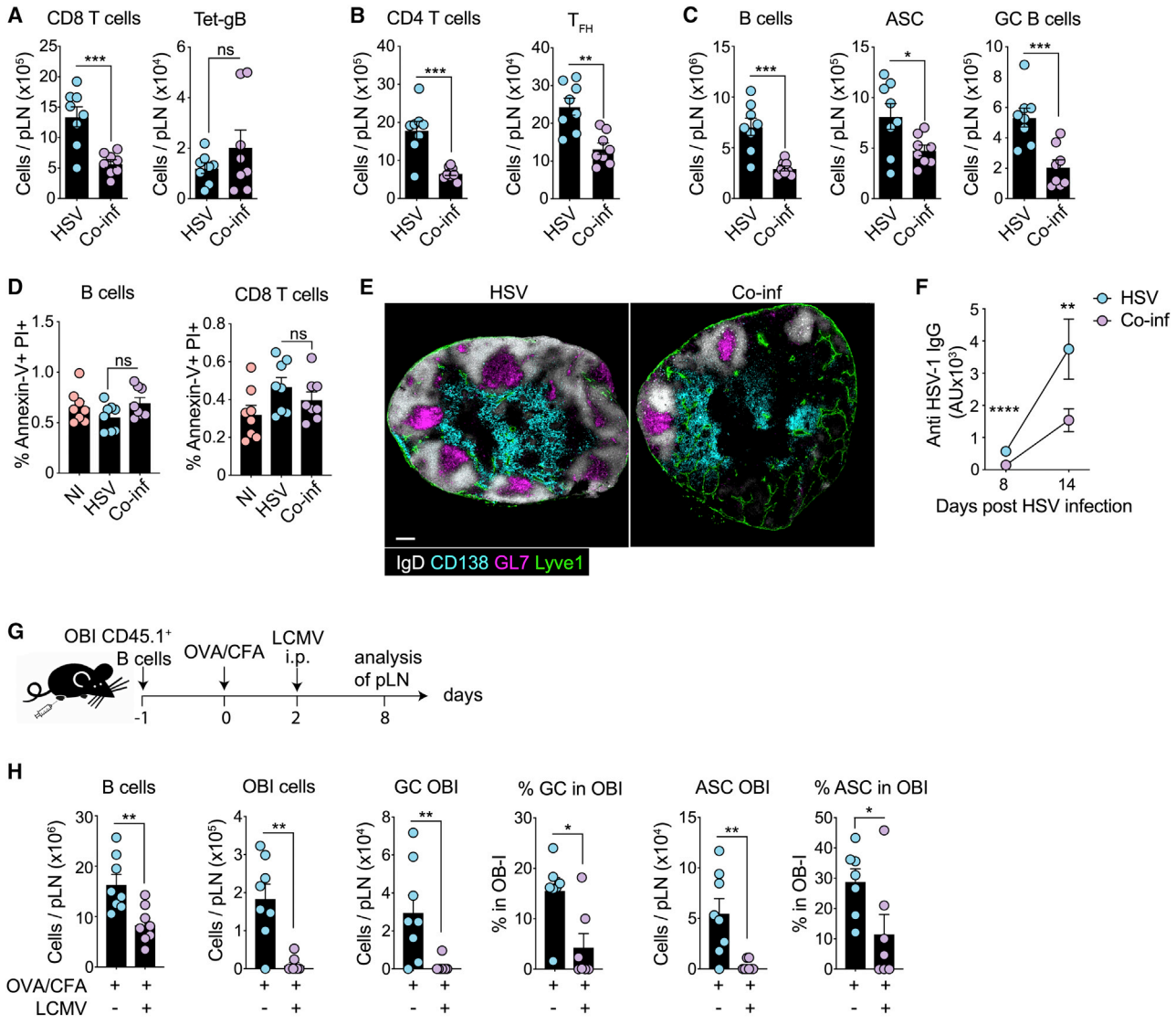

Figure 4. Systemic Coinfection Suppresses B Cell Responses to Localized Infection

(A–C) Mice were infected with HSV s.c. and 2 days later with LCMV i.p. and pLN analyzed for $CD8^+$ T cells and HSV gB $tetramer^+$ cells (A), $CD4^+$ T cells and $CXCR5^+$ $PD1^+$ $CD4^+$ T_{FH} cells (B), and B cells (C). Graphs show pooled data (mean ± SEM) from 2 independent experiments with 8 mice per group. *$p < 0.05$, ***$p < 0.001$, ****$p < 0.0001$, ns, non-significant, by unpaired two-tailed t test.

(D) Coinfection does not increase lymphocyte cell death. pLNs from HSV and coinfected mice were harvested 5 days post-infection and analyzed for annexin V and PI expression on B and $CD8^+$ T cells by flow cytometry. Inguinal LNs from naive mice were included as controls. Graphs show pooled data (mean ± SEM) from 2 independent experiments with 8 mice per group. ns, non-significant, by unpaired two-tailed t test.

(E) pLN sections from NI, HSV, or LCMV infected mice were stained for IgD, CD138, GL7, and Lyve1 and analyzed by confocal microscopy. Data are representative of 2 experiments with 6 mice per group. Scale bar, 200 μm.

(F) Serum anti–HSV-1 IgG titer assessed by ELISA. Mice were infected as in (A) and sera harvested at days 8 and 14 post-HSV infection. Graph shows pooled data (mean ± SEM) from 2 independent experiments with 8 mice per group. *$p < 0.05$, **$p < 0.01$, by unpaired two-tailed t test.

(G) Experimental schematic. Mice were given $CD45.1^+$ OBI B cells 1 day prior to footpad immunization with OVA/CFA. Mice were infected with LCMV i.p. 2 days later. pLNs were analyzed 8 days.

(H) OBI B cell response in the pLN. Graphs show pooled data (mean ± SEM) from 2 independent experiments with 8 mice per group. *$p < 0.05$, **$p < 0.01$, by Mann-Whitney test.

See also Figure S3.

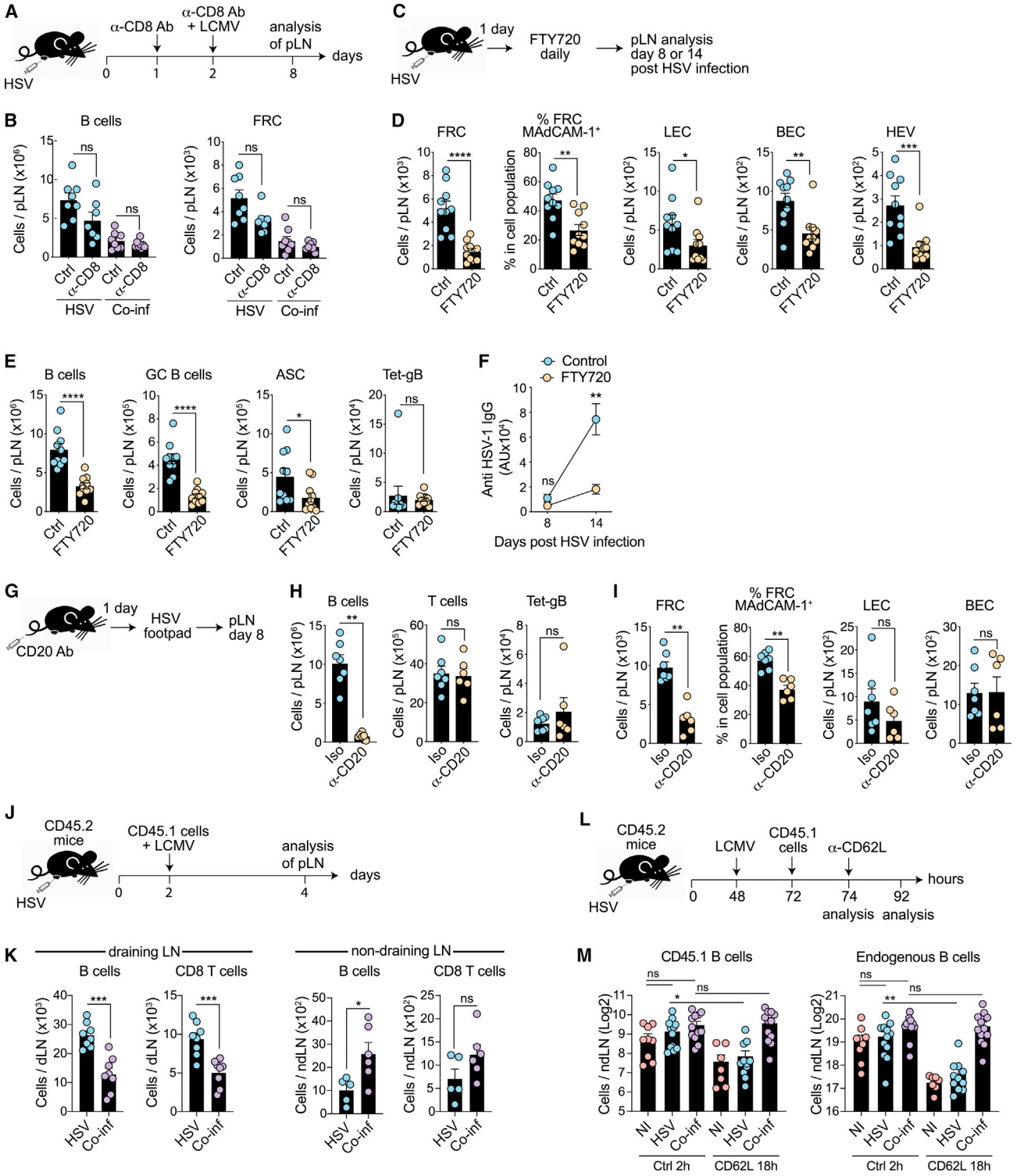

Figure 5. Lymphopenia Induced during Systemic Infection Suppresses Local LN Responses

(A) Experimental schematic of CD8⁺ T cell depletion during coinfection. Mice were infected s.c. with HSV and injected with CD8 depleting antibody on days 1 and 2. Mice were infected with LCMV on day 2. pLNs were analyzed 8 days post HSV infection.

(B) Numbers of B cells and FRC in the pLNs of mice infected with HSV or coinfected with or without CD8⁺ T cells. Graphs show pooled data (mean ± SEM) from 2 independent experiments with 7–8 mice per group. ns, non-significant, by ANOVA with Kruskal-Wallis test.

(C) Experimental schematic of FTY720 treatment during HSV infection. Mice were infected s.c. with HSV and the following day injected i.p. with FTY720 or control for 7 days. pLNs were analyzed 8 days post-HSV infection.

(legend continued on next page)

virus-specific CD8$^+$ T cell responses (Figure 5E). Similarly, blocking lymphocyte homing into pLNs with anti-CD62L antibodies impaired LSC expansion, CD8 T cell responses and B cell numbers 8 days after HSV infection (Figure S4). Antibody responses at day 14 were not reduced by CD62L blockade, as previously described for CD62L-deficient mice (Xu et al., 1996), indicating a role for CD62L-independent mechanisms.

To determine if B cell recruitment was required for expansion of the LNs, we treated mice with an anti-CD20 antibody to deplete B cells prior to HSV infection and examined stromal cell and T cell responses in B cell-ablated mice (Figures 5G–5I). In the absence of B cells, FRC expansion was significantly reduced, and upregulation of MAdCAM-1 by FRCs was blunted, whereas LEC and BEC expansion was unaffected (Figure 5I). T cell recruitment to the HSV-draining pLN and induction of HSV-specific CD8$^+$ T cell responses were unimpaired by depletion of B cells (Figure 5H). Thus, B cells were required to drive FRC expansion in the dLNs during localized viral infection, whereas additional signals contribute to the remodeling of LN endothelial cell compartments.

B Cell Sequestration in Non-draining LNs during Systemic Infection

We next sought to determine if systemic coinfection induced the accumulation of B cells in non-draining LNs (ndLNs). To examine this, we adoptively transferred naive CD45.1$^+$ lymphocytes into HSV and LCMV coinfected mice (Figure 5J). B cell and T cell recruitment to the draining LNs was suppressed, with a concomitant increase in B cell recruitment to ndLNs (Figure 5K). To determine if the increased B cell accumulation in ndLNs resulted from enhanced cell recruitment, cell trapping, or both, we adoptively transferred naive CD45.1$^+$ lymphocytes into HSV and LCMV coinfected mice and assessed B cell numbers in ndLNs 2 h later (Figure 5L). Numbers of CD45.1$^+$ B cells in ndLNs were not significantly increased in LCMV coinfected mice within 2 h of cell transfer when compared to uninfected or HSV-infected mice (Figure 5M), suggesting that cell recruitment to distal LNs was not substantially enhanced by systemic infection. We then treated mice with anti-CD62L blocking antibodies to restrict further cell entry to LNs and determined numbers of B cells remaining in ndLNs 18 h later (Figure 5L). This revealed that B cells that entered ndLNs in LCMV coinfected mice did not egress, whereas cell numbers decreased substantially in uninfected or HSV-infected mice (Figure 5M). We observed similar trapping of endogenous B cells in LCMV coinfected mice. Together, these data show that systemic coinfection sequesters B cells in ndLNs and impairs lymphocyte recruitment to regional dLNs, impairing local LN remodeling.

Systemic Inflammation Suppresses Local Immunity via IFN-I

We hypothesized that systemic inflammation was responsible for the lymphopenia-induced suppression of local LN responses. To examine this, we administered the TLR agonists poly(I:C) or lipopolysaccharide (LPS) to HSV-infected mice (Figure 6A). Both inflammatory mediators substantially reduced the HSV-driven increase in pLN cellularity, FRC expansion, as well as B cell responses (Figure 6B). Systemic LCMV infection induces the production of pro-inflammatory cytokines, including IFN-I (Doughty et al., 2001). LCMV induced a substantial lymphopenia in mice that was dependent on IFN-I receptor (IFNAR) signaling as it did not occur in *Ifnar2*$^{-/-}$ mice (Figure S5A). We asked whether IFNAR signals on B cells contributed to reduced LN hypertrophy and B cell recruitment during coinfection. We generated chimeric mice with a mixture of B cell-deficient (μMT$^{-/-}$) and *Ifnar2*$^{-/-}$ BM to confine the lack of IFNAR expression to B cells (Figure S5B). However, loss of IFNAR in B cells did not restore LN remodeling or B cell responses in coinfected mice (Figure S5C). Examination of reciprocal BM chimeric mice generated by reconstitution of either wild-type (WT) or *Ifnar2*$^{-/-}$ mice with WT or *Ifnar2*$^{-/-}$ BM revealed that cells in both the hematopoietic and non-hematopoietic compartments contributed to altered local LN responses via IFNAR signaling (Figures 6C, S5D, and S5E).

To better define the impact of IFNAR signals on local LN responses, we administered blocking antibodies against IFNAR (anti-IFNAR) to mice infected with HSV or mice coinfected with LCMV in order to reduce IFNAR signals (Figure 6D). Anti-IFNAR treatment did not significantly alter responses in mice infected singly with HSV (Figure 6E). In contrast, anti-IFNAR blockade significantly enhanced the expansion of FRCs, LECs, BECs, and HEV in coinfected mice (Figures 6E and S5F). HSV-specific T cell responses were not altered by anti-IFNAR treatment (Figure 6F), but T and B cell recruitment, GC B cells, and ASC numbers were restored by anti-IFNAR treatment of coinfected

(D and E) Absolute numbers of stromal cell subsets and MAdCAM-1 expression on FRCs (D), and B and T cell responses (E) in pLNs of HSV-infected mice treated with FTY720.

(F) Serum anti-HSV-1 IgG titer assessed by ELISA. Mice were treated as in (C) and sera harvested at days 8 and 14 post-HSV infection. Graphs show pooled data (mean ± SEM) from 2 independent experiments with 10 mice per group for (D) and (E) and 8 mice per group for (F).

(G) Experimental schematic of B cell depletion during HSV infection. Mice were injected i.p. with CD20 depleting antibody and the following day infected s.c. with HSV.

(H and I) Analysis of stromal cells and T cells by flow cytometry in HSV-infected B cell-depleted mice. Graphs show pooled data (mean ± SEM) from 2 independent experiments with 6–7 mice per group.

(J and K) Adoptive transfer of congenic lymphocytes into HSV-infected mice on day 2 and LCMV coinfection, with analysis of CD45.1$^+$ cell numbers in the draining popliteal LNs and non-draining LNs 2 days later. Graphs show pooled data (mean ± SEM) from 2 independent experiments with 5–8 mice per group. *$p < 0.05$, **$p < 0.01$, ***$p < 0.001$, ****$p < 0.0001$, ns, non-significant, by Mann-Whitney test (D, E, G, H, and J).

(L and M) Analysis of early cell recruitment and cell egress. Mice were infected s.c. with HSV, 2 days later coinfected with LCMV i.p., and 24 h later injected i.v. with 8×10^6 CD45.1$^+$ lymphocytes. Mice were harvested 2 h post cell transfer (Ctrl 2 h) or injected with anti-CD62-L blocking antibody and harvested 18 h later. Graphs show pooled data (mean ± SEM) from 3 independent experiments with 7–12 mice per group. *$p < 0.05$, **$p < 0.01$, ns, non-significant, by ANOVA with Kruskal-Wallis test.

See also Figure S4.

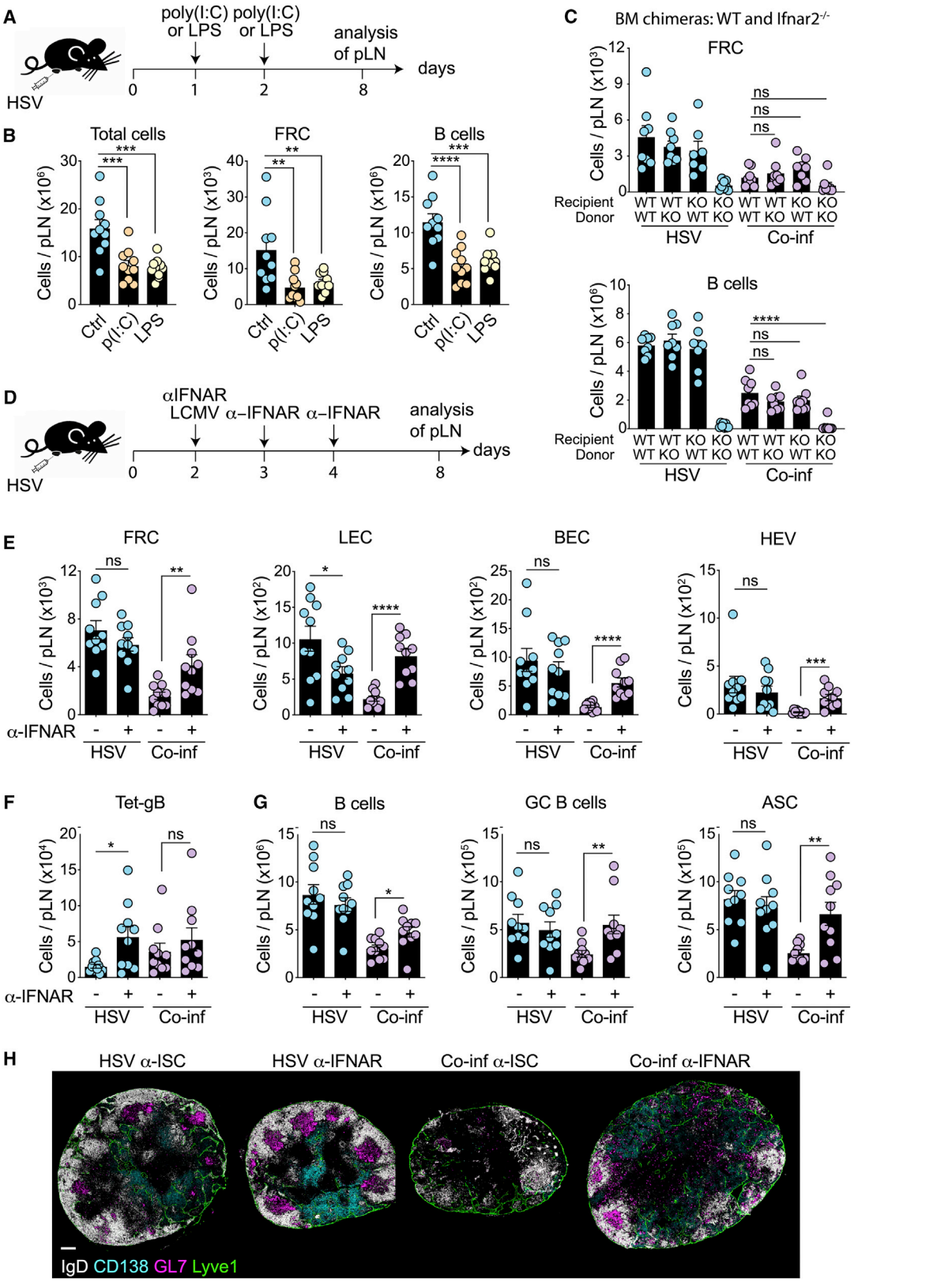

(legend on next page)

mice (Figures 6G and S5F). Microscopy revealed that blocking IFNAR signals improved GC formation and CD138$^+$ plasma cell numbers (Figure 6H). Anti-IFNAR treatment also reduced the sequestration of adoptively transferred B cells in non-draining LNs (Figure S5G). Together, these findings show that systemic inflammation resulted in an IFNAR-dependent lymphopenia that reduced cell recruitment to LN draining the site of local infection and impaired LN remodeling and humoral immunity.

DISCUSSION

Coinfection with multiple pathogens occurs frequently and can alter disease outcomes and subsequent immunity (Mabbott, 2018; Stelekati and Wherry, 2012). Diverse mechanisms likely contribute to altered immunity during pathogen coinfections, yet our understanding of these processes remains incomplete. Here, we show that widespread inflammation triggered by systemic coinfection impairs dLN remodeling and B cell responses during concurrent localized viral infection or immunization. Mechanistically, systemic inflammation results in an IFN-I-dependent lymphopenia and sequestration of lymphocytes in non-draining LNs, which impairs the recruitment of lymphocytes to LN draining sites of peripheral infection, thereby contributing to constrained local humoral immunity.

Recruitment of lymphocytes to inflamed LNs triggers LN expansion in response to infection or immunization (Gregory et al., 2017; Yang et al., 2014). This requires circulating lymphocytes as a source of cells to feed the draining LN. Systemic infections (including malaria and COVID-19) and autoimmune diseases (including systemic lupus erythematosus [SLE]) can induce lymphopenia, resulting in the trapping of lymphocytes in secondary lymphoid organs around the body, thereby reducing the circulating pool of lymphocytes. We show that induction of lymphopenia during systemic infection, inflammation or following FTY720 treatment impairs draining LN responses. B cells can coordinate the expansion of the lymphatic network in LNs during inflammation (Angeli et al., 2006; Kumar et al., 2010). We show that removal of B cells impaired the expansion and activation of FRC but had little impact on expansion of LECs or BECs during local HSV infection. The reason for this difference is unclear but may reflect the ability of both CD4$^+$ and CD8$^+$ T cells to also support LN expansion and remodeling (Gregory et al., 2017).

Our results show that concurrent systemic inflammation impaired lymphocyte recruitment and LN remodeling, which restrained B cell responses but did not impact CTL responses. It is worth noting that single infection with LCMV resulted in smaller LNs and fewer B cells than co-infected mice, indicating that the local response was not entirely suppressed by systemic infection. LN hypertrophy peaks 1–2 weeks after infection, whereas T cells are activated and leave the draining LNs within 1 week (Hor et al., 2015). Conversely, B cells require a prolonged period of activation and maturation within LNs in order to form antibody secreting plasma cells and long-lived memory B cells (Cyster and Allen, 2019). This indicates that lymphadenopathy may be critical for the support of B cell responses, probably to support GC reactions and memory B cell formation in the dLNs. In support of this, we also observed reduced numbers of T_{FH} cells in coinfected mice.

We show that recruitment of cells to the dLNs and expansion of LSC during infection requires IFNAR signaling, and this was absent in mice where both hematopoietic and non-hematopoietic cells lacked IFNAR. Type I IFN play numerous homeostatic roles, and complete loss of signaling in IFNAR$^{-/-}$ mice might confound interpretation of its role in modulating responses (Gough et al., 2012). However, by reducing the abundant systemic IFN-I signals induced during LCMV co-infection following treatment with anti-IFNAR blocking antibody, we reveal that cell recruitment to the draining LN and B cell responses were improved. Thus, reducing, but not abrogating, systemic inflammatory signals was important for restoring the local LN response. Notably, we did not find a role for direct IFNAR signaling in B cells, which supports a previous study showing that IFNAR$^{-/-}$ B cells did not show increased migration to LN during lymphopenia (Kamphuis et al., 2006). In contrast, extrinsic IFNAR signals influence B cell accumulation in inflamed LNs (Hastey et al., 2014). Whether IFNAR signaling results in the production of other inflammatory mediators (such as interleukin [IL]-6) that further contribute to the sequestration of lymphocytes requires further investigation.

Many medically important pathogens cause acute or persistent systemic infections, and evidence suggests that immunity to vaccination or challenge with unrelated pathogens is often impaired during coinfection (Griffiths et al., 2011; Stelekati and Wherry, 2012). Models of viral and bacterial coinfection have revealed increased susceptibility to infection and altered

Figure 6. Systemic Inflammation Suppresses Local Immunity via IFN-I

(A) Experimental schematic of adjuvant injection in HSV-infected mice. Mice were infected s.c. with HSV and 2 d later received 2 i.p. injections of either poly(I:C) or LPS 24 h apart. pLNs were harvested 8 d post-HSV infection.

(B) Numbers of total cells, FRCs and B cells analyzed by flow cytometry in infected mice injected with poly(I:C) or LPS. Graphs show pooled data (mean ± SEM) from 2 independent experiments with 10 mice per group.

(C) Cell numbers in the pLNs of HSV and coinfected WT and *Ifnar2*$^{-/-}$ BM chimeric mice. Graphs show pooled data (mean ± SEM) from two independent experiments. *p < 0.05, **p < 0.01, ***p < 0.001, ns, non-significant, by ANOVA with Kruskal-Wallis test.

(D) Experimental schematic of IFNAR blocking during HSV and coinfection. Mice were infected s.c. with HSV, infected i.p. with LCMV on day 2 and injected with anti-IFNAR blocking antibody or isotype control (ISC) antibody on days 2–4. Mice were analyzed on 8 days post-HSV infection.

(E–G) Analysis of cellularity of stromal cell subsets (E), HSV-specific CD8$^+$ T cells (F), and B cell response (G) in the pLNs of HSV and coinfected mice during IFNAR blocking. Graphs show pooled data (mean ± SEM) from 2 independent experiments with 10 mice per group. *p < 0.05, **p < 0.01, ****p < 0.0001, ns, non-significant, by unpaired two-tailed t test.

(H) pLN sections from mice treated with anti-IFNAR blocking antibody or ISC were stained for IgD, CD138, GL7, and Lyve1 and analyzed by confocal microscopy. Data are representative of 2 experiments with 4 mice per group. Scale bar, 200 μm.

See also Figure S5.

responses. During the early stage of LCMV infection, IFN-I sensitizes mice to bacterial endotoxin (Doughty et al., 2001; Nansen and Randrup Thomsen, 2001), which can lead to NK cell-mediated impairment of the $CD8^+$ T cell responses (Straub et al., 2018). Coinfection of mice with two systemic viral pathogens, LCMV and Ectromelia virus (McAfee et al., 2015) or LCMV and Pichinde virus, was also found to impair $CD8^+$ T cell responses to LCMV (Kenney et al., 2015). In our experiments, LCMV coinfection did not inhibit HSV-specific $CD8^+$ T cell responses but rather impaired the induction of local B cell responses. In humans, coinfection may both directly and indirectly affect B cell differentiation and antibody production (Stelekati and Wherry, 2012). Bacterial coinfection of mice with *Streptococcus pneumoniae* was shown to either enhance or inhibit B cell responses to influenza virus depending on the timing of respiratory coinfection (Wu et al., 2015). During the early phase of chronic LCMV clone-13 infection, virus-specific B cell responses can be inhibited by IFN-I production that results in death of activated B cells and induction of short-lived ASCs at the expense of sustained neutralizing antibody responses (Fallet et al., 2016; Moseman et al., 2016; Sammicheli et al., 2016). Coinfection with VSV and LCMV clone-13 in the footpad was also shown to restrict antigen-specific B cell responses (Sammicheli et al., 2016). Other viruses can also interfere with B cell responses (Kuka and Iannacone, 2018), including Chikungunya virus infection that has been shown to recruit monocytes and neutrophils that impair LN B cell responses (McCarthy et al., 2020).

Here, we reveal a mechanism by which infection can indirectly interfere with B cell responses. We show that systemic inflammation induced by LCMV infection, the TLR3 agonist Poly(I:C), or the endotoxin LPS induced a lymphopenia that reduced the recruitment of lymphocytes to the dLN during localized infection. This suppression of dLN swelling, stromal cell expansion, and B cell immunity suggests that opportunistic localized infections might be harder to eradicate in hosts undergoing systemic inflammatory reactions. Both infectious and non-infectious systemic inflammatory reactions might suppress regional immunity when occurring contemporaneously. In contrast, latent coinfection with murine gammaherpesvirus 68 or murine cytomegalovirus was shown to protect against bacterial infection (Barton et al., 2007), at least transiently (Yager et al., 2009), due to the systemic production of low levels of cytokines. This indicates that the magnitude of systemic inflammation plays important roles in influencing the outcomes of concomitant regional immune responses.

Overall, our data show that systemic inflammation impacts the host's ability to mount immune responses in LN draining the site of a localized challenge by impairing cell recruitment and restricting tissue remodeling and B cell responses. The prevalence of coinfections in people suggests that it will be important to better define how systemic inflammatory responses in humans impact regional immunity and the progression of diseases that are initiated in barrier tissues.

STAR★METHODS

Detailed methods are provided in the online version of this paper and include the following:

SUPPLEMENTAL INFORMATION

Supplemental Information can be found online at https://doi.org/10.1016/j.celrep.2020.108567.

ACKNOWLEDGMENTS

We thank Paul Hertzog (Hudson Institute, Australia) for anti-IFNAR antibody, Hidde Ploegh (Whitehead Institute, Cambridge, MA) for OBI mice, Genentech for anti-mouse CD20 antibody, the Biological Optical Microscopy Platform (BOMP) for support, and Yu Kato for advice on HSV ELISA. This work was supported by the National Health and Medical Research Council of Australia and the Australian Research Council (to L.K.M., W.R.H., and S.N.M.).

AUTHOR CONTRIBUTIONS

Conceptualization, Y.O.A. and S.N.M.; Methodology, Y.O.A. and S.D.; Investigation, Y.O.A., S.D., and S.L.P.; Writing, Y.O.A. and S.N.M.; Resources, L.K.M. and W.R.H.; Visualization, Y.O.A. and S.N.M.; Funding Acquisition, S.N.M.

DECLARATION OF INTERESTS

The authors declare no competing interests.

Received: July 10, 2020
Revised: November 9, 2020
Accepted: December 7, 2020
Published: December 29, 2020

REFERENCES

Alexandre, Y.O., and Mueller, S.N. (2018). Stromal cell networks coordinate immune response generation and maintenance. Immunol. Rev. *283*, 77–85.

Angeli, V., Ginhoux, F., Llodrà, J., Quemeneur, L., Frenette, P.S., Skobe, M., Jessberger, R., Merad, M., and Randolph, G.J. (2006). B cell-driven lymphangiogenesis in inflamed lymph nodes enhances dendritic cell mobilization. Immunity *24*, 203–215.

Barton, E.S., White, D.W., Cathelyn, J.S., Brett-McClellan, K.A., Engle, M., Diamond, M.S., Miller, V.L., and Virgin, H.W., 4th. (2007). Herpesvirus latency confers symbiotic protection from bacterial infection. Nature *447*, 326–329.

Borrow, P., Evans, C.F., and Oldstone, M.B. (1995). Virus-induced immunosuppression: immune system-mediated destruction of virus-infected dendritic cells results in generalized immune suppression. J. Virol. *69*, 1059–1070.

Chang, C.C., Crane, M., Zhou, J., Mina, M., Post, J.J., Cameron, B.A., Lloyd, A.R., Jaworowski, A., French, M.A., and Lewin, S.R. (2013). HIV and co-infections. Immunol. Rev. *254*, 114–142.

Cremasco, V., Woodruff, M.C., Onder, L., Cupovic, J., Nieves-Bonilla, J.M., Schildberg, F.A., Chang, J., Cremasco, F., Harvey, C.J., Wucherpfennig, K., et al. (2014). B cell homeostasis and follicle confines are governed by fibroblastic reticular cells. Nat. Immunol. *15*, 973–981.

Cyster, J.G., and Allen, C.D.C. (2019). B Cell Responses: Cell Interaction Dynamics and Decisions. Cell *177*, 524–540.

Davies, B., Prier, J.E., Jones, C.M., Gebhardt, T., Carbone, F.R., and Mackay, L.K. (2017). Cutting Edge: Tissue-Resident Memory T Cells Generated by Multiple Immunizations or Localized Deposition Provide Enhanced Immunity. J. Immunol. *198*, 2233–2237.

Denton, A.E., Roberts, E.W., Linterman, M.A., and Fearon, D.T. (2014). Fibroblastic reticular cells of the lymph node are required for retention of resting but not activated CD8+ T cells. Proc. Natl. Acad. Sci. USA *111*, 12139–12144.

Dougan, S.K., Ogata, S., Hu, C.C., Grotenbreg, G.M., Guillen, E., Jaenisch, R., and Ploegh, H.L. (2012). IgG1+ ovalbumin-specific B-cell transnuclear mice show class switch recombination in rare allelically included B cells. Proc. Natl. Acad. Sci. USA *109*, 13739–13744.

Doughty, L., Nguyen, K., Durbin, J., and Biron, C. (2001). A role for IFN-alpha beta in virus infection-induced sensitization to endotoxin. J. Immunol. *166*, 2658–2664.

Edwards, C.L., Zhang, V., Werder, R.B., Best, S.E., Sebina, I., James, K.R., Faleiro, R.J., de Labastida Rivera, F., Amante, F.H., Engwerda, C.R., et al. (2015). Coinfection with Blood-Stage Plasmodium Promotes Systemic Type I Interferon Production during Pneumovirus Infection but Impairs Inflammation and Viral Control in the Lung. Clin. Vaccine Immunol. *22*, 477–483.

Fallet, B., Narr, K., Ertuna, Y.I., Remy, M., Sommerstein, R., Cornille, K., Kreutzfeldt, M., Page, N., Zimmer, G., Geier, F., et al. (2016). Interferon-driven deletion of antiviral B cells at the onset of chronic infection. Sci. Immunol. *1*, eaah6817.

Gough, D.J., Messina, N.L., Clarke, C.J., Johnstone, R.W., and Levy, D.E. (2012). Constitutive type I interferon modulates homeostatic balance through tonic signaling. Immunity *36*, 166–174.

Gregory, J.L., Walter, A., Alexandre, Y.O., Hor, J.L., Liu, R., Ma, J.Z., Devi, S., Tokuda, N., Owada, Y., Mackay, L.K., et al. (2017). Infection Programs Sustained Lymphoid Stromal Cell Responses and Shapes Lymph Node Remodeling upon Secondary Challenge. Cell Rep. *18*, 406–418.

Griffiths, E.C., Pedersen, A.B., Fenton, A., and Petchey, O.L. (2011). The nature and consequences of coinfection in humans. J. Infect. *63*, 200–206.

Halin, C., Scimone, M.L., Bonasio, R., Gauguet, J.M., Mempel, T.R., Quackenbush, E., Proia, R.L., Mandala, S., and von Andrian, U.H. (2005). The S1P-analog FTY720 differentially modulates T-cell homing via HEV: T-cell-expressed S1P1 amplifies integrin activation in peripheral lymph nodes but not in Peyer patches. Blood *106*, 1314–1322.

Hastey, C.J., Ochoa, J., Olsen, K.J., Barthold, S.W., and Baumgarth, N. (2014). MyD88- and TRIF-independent induction of type I interferon drives naive B cell accumulation but not loss of lymph node architecture in Lyme disease. Infect. Immun. *82*, 1548–1558.

Hor, J.L., Whitney, P.G., Zaid, A., Brooks, A.G., Heath, W.R., and Mueller, S.N. (2015). Spatiotemporally Distinct Interactions with Dendritic Cell Subsets Facilitates CD4+ and CD8+ T Cell Activation to Localized Viral Infection. Immunity *43*, 554–565.

Hotchkiss, R.S., Monneret, G., and Payen, D. (2013). Sepsis-induced immunosuppression: from cellular dysfunctions to immunotherapy. Nat. Rev. Immunol. *13*, 862–874.

Huang, H.Y., Rivas-Caicedo, A., Renevey, F., Cannelle, H., Peranzoni, E., Scarpellino, L., Hardie, D.L., Pommier, A., Schaeuble, K., Favre, S., et al. (2018). Identification of a new subset of lymph node stromal cells involved in regulating plasma cell homeostasis. Proc. Natl. Acad. Sci. USA *115*, E6826–E6835.

Jones, C.M., Cose, S.C., Coles, R.M., Winterhalter, A.C., Brooks, A.G., Heath, W.R., and Carbone, F.R. (2000). Herpes simplex virus type 1-specific cytotoxic T-lymphocyte arming occurs within lymph nodes draining the site of cutaneous infection. J. Virol. *74*, 2414–2419.

Kamphuis, E., Junt, T., Waibler, Z., Forster, R., and Kalinke, U. (2006). Type I interferons directly regulate lymphocyte recirculation and cause transient blood lymphopenia. Blood *108*, 3253–3261.

Kenney, L.L., Cornberg, M., Chen, A.T., Emonet, S., de la Torre, J.C., and Selin, L.K. (2015). Increased Immune Response Variability during Simultaneous Viral Coinfection Leads to Unpredictability in CD8 T Cell Immunity and Pathogenesis. J. Virol. *89*, 10786–10801.

Kuka, M., and Iannacone, M. (2018). Viral subversion of B cell responses within secondary lymphoid organs. Nat. Rev. Immunol. *18*, 255–265.

Kumar, V., Scandella, E., Danuser, R., Onder, L., Nitschké, M., Fukui, Y., Halin, C., Ludewig, B., and Stein, J.V. (2010). Global lymphoid tissue remodeling during a viral infection is orchestrated by a B cell-lymphotoxin-dependent pathway. Blood *115*, 4725–4733.

Langhorne, P., Stott, D.J., Robertson, L., MacDonald, J., Jones, L., McAlpine, C., Dick, F., Taylor, G.S., and Murray, G. (2000). Medical complications after stroke: a multicenter study. Stroke *31*, 1223–1229.

Leist, T.P., Rüedi, E., and Zinkernagel, R.M. (1988). Virus-triggered immune suppression in mice caused by virus-specific cytotoxic T cells. J. Exp. Med. *167*, 1749–1754.

Mabbott, N.A. (2018). The Influence of Parasite Infections on Host Immunity to Co-infection With Other Pathogens. Front. Immunol. *9*, 2579.

Malhotra, D., Fletcher, A.L., Astarita, J., Lukacs-Kornek, V., Tayalia, P., Gonzalez, S.F., Elpek, K.G., Chang, S.K., Knoblich, K., Hemler, M.E., et al.; Immunological Genome Project Consortium (2012). Transcriptional profiling of stroma from inflamed and resting lymph nodes defines immunological hallmarks. Nat. Immunol. *13*, 499–510.

McAfee, M.S., Huynh, T.P., Johnson, J.L., Jacobs, B.L., and Blattman, J.N. (2015). Interaction between unrelated viruses during in vivo co-infection to limit pathology and immunity. Virology *484*, 153–162.

McCarthy, M.K., Reynoso, G.V., Winkler, E.S., Mack, M., Diamond, M.S., Hickman, H.D., and Morrison, T.E. (2020). MyD88-dependent influx of monocytes and neutrophils impairs lymph node B cell responses to chikungunya virus infection via Irf5, Nos2 and Nox2. PLoS Pathog. *16*, e1008292.

Moseman, E.A., Wu, T., de la Torre, J.C., Schwartzberg, P.L., and McGavern, D.B. (2016). Type I interferon suppresses virus-specific B cell responses by modulating $CD8^+$ T cell differentiation. Sci. Immunol. *1*, eaah3565.

Mueller, S.N., and Germain, R.N. (2009). Stromal cell contributions to the homeostasis and functionality of the immune system. Nat. Rev. Immunol. *9*, 618–629.

Mueller, S.N., Hosiawa-Meagher, K.A., Konieczny, B.T., Sullivan, B.M., Bachmann, M.F., Locksley, R.M., Ahmed, R., and Matloubian, M. (2007a). Regulation of homeostatic chemokine expression and cell trafficking during immune responses. Science *317*, 670–674.

Mueller, S.N., Matloubian, M., Clemens, D.M., Sharpe, A.H., Freeman, G.J., Gangappa, S., Larsen, C.P., and Ahmed, R. (2007b). Viral targeting of fibroblastic reticular cells contributes to immunosuppression and persistence during chronic infection. Proc. Natl. Acad. Sci. USA *104*, 15430–15435.

Nansen, A., and Randrup Thomsen, A. (2001). Viral infection causes rapid sensitization to lipopolysaccharide: central role of IFN-alpha beta. J. Immunol. *166*, 982–988.

Odermatt, B., Eppler, M., Leist, T.P., Hengartner, H., and Zinkernagel, R.M. (1991). Virus-triggered acquired immunodeficiency by cytotoxic T-cell-dependent destruction of antigen-presenting cells and lymph follicle structure. Proc. Natl. Acad. Sci. USA *88*, 8252–8256.

Olson, M.R., McDermott, D.S., and Varga, S.M. (2012). The initial draining lymph node primes the bulk of the CD8 T cell response and influences memory T cell trafficking after a systemic viral infection. PLoS Pathog. *8*, e1003054.

Roost, H., Charan, S., Gobet, R., Rüedi, E., Hengartner, H., Althage, A., and Zinkernagel, R.M. (1988). An acquired immune suppression in mice caused by infection with lymphocytic choriomeningitis virus. Eur. J. Immunol. *18*, 511–518.

Sammicheli, S., Kuka, M., Di Lucia, P., de Oya, N.J., De Giovanni, M., Fioravanti, J., Cristofani, C., Maganuco, C.G., Fallet, B., Ganzer, L., et al. (2016). Inflammatory monocytes hinder antiviral B cell responses. Sci. Immunol. *1*, eaah6789.

Shiow, L.R., Rosen, D.B., Brdicková, N., Xu, Y., An, J., Lanier, L.L., Cyster, J.G., and Matloubian, M. (2006). CD69 acts downstream of interferon-alpha/beta to inhibit S1P1 and lymphocyte egress from lymphoid organs. Nature *440*, 540–544.

Stelekati, E., and Wherry, E.J. (2012). Chronic bystander infections and immunity to unrelated antigens. Cell Host Microbe *12*, 458–469.

Straub, T., Freudenberg, M.A., Schleicher, U., Bogdan, C., Gasteiger, G., and Pircher, H. (2018). Bacterial coinfection restrains antiviral CD8 T-cell response via LPS-induced inhibitory NK cells. Nat. Commun. *9*, 4117.

Wu, Y., Tu, W., Lam, K.T., Chow, K.H., Ho, P.L., Guan, Y., Peiris, J.S., and Lau, Y.L. (2015). Lethal coinfection of influenza virus and Streptococcus pneumoniae lowers antibody response to influenza virus in lung and reduces numbers of germinal center B cells, T follicular helper cells, and plasma cells in mediastinal lymph Node. J. Virol. *89*, 2013–2023.

Xu, J., Grewal, I.S., Geba, G.P., and Flavell, R.A. (1996). Impaired primary T cell responses in L-selectin-deficient mice. J. Exp. Med. *183*, 589–598.

Yager, E.J., Szaba, F.M., Kummer, L.W., Lanzer, K.G., Burkum, C.E., Smiley, S.T., and Blackman, M.A. (2009). gamma-Herpesvirus-induced protection against bacterial infection is transient. Viral Immunol. *22*, 67–72.

Yang, C.Y., Vogt, T.K., Favre, S., Scarpellino, L., Huang, H.Y., Tacchini-Cottier, F., and Luther, S.A. (2014). Trapping of naive lymphocytes triggers rapid growth and remodeling of the fibroblast network in reactive murine lymph nodes. Proc. Natl. Acad. Sci. USA *111*, E109–E118.

STAR★METHODS

KEY RESOURCES TABLE

REAGENT or RESOURCE	SOURCE	IDENTIFIER
Antibodies		
Pacific Blue anti-mouse/human CD45R/B220 Antibody	Biolegend	Cat# 103227, RRID:AB_492876
PE/Cy7 anti-mouse/human CD45R/B220 antibody	Biolegend	Cat# 103221, RRID:AB_313004
Alexa Fluor® 700 anti-mouse/human CD45R/B220 antibody	Biolegend	Cat# 103232, RRID:AB_493717
Rat Anti-Mouse CD138 Monoclonal Antibody, PE Conjugated, Clone 281-2	BD Biosciences	Cat# 561070, RRID:AB_2033998
APC anti-mouse CD157 (BST-1) antibody	Biolegend	Cat# 140208, RRID:AB_10901172
Alexa Fluor® 647 anti-mouse CD138 (Syndecan-1) antibody	Biolegend	Cat# 142525, RRID:AB_2566238
BV650 Mouse Anti-Mouse CD157 Clone BP-3	BD Biosciences	Cat# 740611, RRID:AB_2740311
Rat Anti-CD19 Monoclonal Antibody, PerCP-Cy5.5 Conjugated, Clone 1D3	BD Biosciences	Cat# 551001, RRID:AB_394004
BV605 Rat Anti-Mouse CD19 antibody	BD Biosciences	Cat# 563148, RRID:AB_2732057
Brilliant Violet 421 anti-mouse CD31 antibody	Biolegend	Cat# 102423, RRID:AB_2562186
PE/Cy7 anti-mouse CD31 antibody,	Biolegend	Cat# 102417, RRID:AB_830756
Alexa Fluor(R) 647 anti-mouse CD31 antibody,	Biolegend	Cat# 102516, RRID:AB_2161029
PE/Cy7 anti-mouse CD38 antibody	Biolegend	Cat# 102717, RRID:AB_2072892
CD3e Monoclonal Antibody (eBio500A2 (500A2)), Alexa Fluor 700	ThermoFisher	Cat# 56-0033-80, RRID:AB_837092
Brilliant Violet 605 anti-mouse CD4 antibody,	Biolegend	Cat# 100547, RRID:AB_11125962
Rat Anti-CD4 Monoclonal Antibody, PE-Cy7 Conjugated, Clone RM4-5	BD Biosciences	Cat# 552775, RRID:AB_394461
Rat Anti-CD4 Monoclonal Antibody, Allophycocyanin Conjugated, Clone RM4-5	BD Biosciences	Cat# 553051, RRID:AB_398528
Alexa Fluor® 700 anti-mouse CD45 antibody	Biolegend	Cat# 147716, RRID:AB_2750449
Brilliant Violet 785 anti-mouse CD8a antibody	Biolegend	Cat# 100750, RRID:AB_2562610
APC anti-mouse CD8a antibody,	Biolegend	Cat# 100712, RRID:AB_312751
BV786 Rat Anti-Mouse CD8b Clone H35-17.2	BD Biosciences	Cat# 740952, RRID:AB_2740577
CD185 (CXCR5) Monoclonal Antibody (SPRCL5), Biotin, eBioscience	ThermoFischer	Cat# 13-7185-82, RRID:AB_2572800
rat anti mouse follicular dendritic cells mAb clone FDC-M2	AMSBIO	Cat# 212-MK-1FDCM2, RRID:AB_10920049
Alexa Fluor(R) 647 anti-MU/HU GL7 Antigen (T/B Cell Act. Marker) antibody	Biolegend	Cat# 144605, RRID:AB_2562184
Pacific Blue(TM) anti-MU/HU GL7 Antigen (T/B Cell Act. Marker) antibody	Biolegend	Cat# 144614, RRID:AB_2563292
Alexa Fluor® 594 anti-mouse IgD antibody	Biolegend	Cat# 405740, RRID:AB_2565572
Ki-67 Monoclonal Antibody (SolA15), eFluor 660, eBioscience	ThermoFischer	Cat# 50-5698-82, RRID:AB_2574235
Rabbit Anti-Laminin Polyclonal Antibody, Unconjugated	Abcam	Cat# ab11575, RRID:AB_298179
InVivoMab anti-LCMV nucleoprotein antibody	Bio X cell	Cat# BE0106, RRID:AB_10949017
Rabbit Anti-LYVE1 Polyclonal Antibody, Unconjugated	Abcam	Cat# ab14917, RRID:AB_301509
Biotin anti-mouse MAdCAM-1 antibody	Biolegend	Cat# 120706, RRID:AB_493397
Purified anti-mouse MAdCAM-1 antibody	Biolegend	Cat# 120702, RRID:AB_493393

(*Continued on next page*)

Continued

REAGENT or RESOURCE	SOURCE	IDENTIFIER
High Endothelial Venule Marker Monoclonal Antibody (MECA-79), Alexa Fluor 488, eBioscience	ThermoFischer	Cat# 53-6036-82, RRID:AB_10804391
Podoplanin Monoclonal Antibody (eBio8.1.1 (8.1.1)), PE, eBioscience	ThermoFischer	Cat# 12-5381-80, RRID:AB_1907440
Podoplanin Monoclonal Antibody (eBio8.1.1 (8.1.1)), Alexa Fluor 488, eBioscience	ThermoFischer	Cat# 53-5381-82, RRID:AB_1106990
PE/Cy7 anti-mouse Podoplanin antibody	Biolegend	Cat# 127411, RRID:AB_10613294
Purified anti-mouse Podoplanin antibody	Biolegend	Cat# 127401, RRID:AB_1089186
CD254 (RANK Ligand) Monoclonal Antibody (IK22/5), Biotin, eBioscience	ThermoFischer	Cat# 13-5952-82, RRID:AB_466813
Streptavidin, Alexa Fluor® 555 conjugate antibody	ThermoFischer	Cat# s21381, RRID:AB_2307336
Streptavidin-Allophycocyanin antibody	BD Biosciences	Cat# 554067, RRID:AB_10050396
PE-Cy7 Streptavidin	BD Biosciences	Cat# 557598
Brilliant Violet 711 Streptavidin	Biolegend	Cat# 405241
BV711 TCR β Chain antibody,	BD Biosciences	Cat# 563135, RRID:AB_2738023
Armenian Hamster Anti-TCR beta Monoclonal Antibody, FITC Conjugated, Clone H57-597	BD Biosciences	Cat# 553171, RRID:AB_394683
TER-119 Monoclonal Antibody (TER-119), PerCP-Cyanine5.5, eBioscience	ThermoFischer	Cat# 45-5921-82, RRID:AB_925765
Alexa Fluor® 700 anti-mouse TER-119/Erythroid Cells antibody	Biolegend	Cat# 116220, RRID:AB_528963
PerCP/Cyanine5.5 anti-mouse CD21/CD35 (CR2/CR1) antibody	Biolegend	Cat# 123416, RRID:AB_1595490
Goat anti-Hamster IgG (H+L) Cross-Adsorbed Secondary Antibody, Alexa Fluor 647	ThermoFischer	Cat# A-21451, RRID:AB_2535868
Goat Anti-Rabbit IgG (H+L) Antibody, Alexa Fluor 488 Conjugated	ThermoFischer	Cat# A-11008, RRID:AB_143165
Goat anti-Rabbit IgG (H+L) Highly Cross-Adsorbed Secondary Antibody, Alexa Fluor 594	ThermoFischer	Cat# A-11037, RRID:AB_2534095
Goat anti-Rat IgG (H+L) Cross-Adsorbed Secondary Antibody, Alexa Fluor 594	ThermoFischer	Cat# A-11007, RRID:AB_10561522
InVivoMab anti-mouse IFNAR-1 antibody	Bio X Cell	Cat# BE0241, RRID:AB_2687723
anti-mouse IFNAR-1 antibody (MAR-1 clone)	Gift from Paul Hertzog	N/A
InVivoMab mouse IgG1 isotype control antibody	Bio X Cell	Cat# BE0083, RRID:AB_1107784
InVivoMab anti-mouse CD8α antibody	Bio X Cell	Cat# BE0117, RRID:AB_10950145
Anti mouse CD20, clone 5D2	Genenteck	N/A
InVivoMab anti-mouse L-Selectin (CD62L) antibody	Bio X Cell	Cat# BE0021, RRID:AB_1107665
Donkey anti-Mouse IgG (H+L) Secondary Antibody, HRP	ThermoFischer	Cat# A16011, RRID:AB_2534685
Bacterial and Virus Strains		
Herpes Simplex virus type-1 (HSV-1), KOS strain	In-house	N/A
Lymphocytic choriomeningitis virus, Armstrong strain	In-house	N/A
recombinant Influenza A H3N2, strain X31, expressing the HSV glycoprotein-B-derived epitope $gB_{498–505}$	In-house	N/A
Biological Samples		
Bovine serum albumin	Sigma-Aldrich	Cat# A7906
Foetal Bovine serum	Sigma-Aldrich	N/A
Albumin from chicken egg white	Sigma-Aldrich	A5503
Chemicals, Peptides, and Recombinant Proteins		
K^b-gB tetramers	GenScript	Cat# RP19992

(*Continued on next page*)

Continued

REAGENT or RESOURCE	SOURCE	IDENTIFIER
T-Select H-2D^{b} LCMV gp33 Tetramer-KAVYNFATC-PE	MBL International	TB-5002-1
Trypsin/EDTA solution	Sigma-Aldrich	Cat# T4049
EDTA	Sigma-Aldrich	Cat# E5134
Sphero calibration particles	BD Bioscience	Cat# 556296
16% Paraformaldehyde Aqueous solution, EM grade	Electron Microscopy Sciences	Cat# 15710
Collagenase D	Sigma Aldrich	COLLD-RO
DISPASE II (NEUTRAL PROTEASE GRADE II)	Sigma Aldrich	4942078001
Deoxyribonuclease I from bovine pancreas	Sigma Aldrich	DN25
o-Phenylenediamine	Sigma Aldrich	P23938
MitoTracker Deep Red FM	ThermoFisher	M22426
BODIPY FL C_{16} (4,4-Difluoro-5,7-Dimethyl-4-Bora-3a,4a-Diaza-*s*-Indacene-3-Hexadecanoic Acid)	ThermoFisher	D3821
CellROX Orange Reagent	ThermoFisher	C10443
2-NBDG (2-(*N*-(7-Nitrobenz-2-oxa-1,3-diazol-4-yl) Amino)-2-Deoxyglucose)	ThermoFisher	N13195
RPMI 1640 Medium, no glucose	ThermoFisher	11879020
FTY720 (S)-Phosphate	Caymanchem	402616-26-6
cyclodextrin	Sigma	
Poly(I:C) HMW	InvivoGen	tlrl-pic
LPS-EB Ultrapure	InvivoGen	tlrl-3pelps
Freund's Adjuvant, Complete,cell suspension	Sigma Aldrich	F5881-10ML
OCT Embedding Compound 4oz Tissue-Tek	Trajan Scientific	4583
Protein Block, Serum-Free	Agilent	X0909
ProLong Gold Antifade Mountant	ThermoFisher	P10144
HSV-1 (MacIntyre Strain) Inactivated Vero Cell Extract	Advanced biotechnologies	10-515-001
Critical Commercial Assays		
Live/dead fixable Near-IR Dead Cell Stain Kit	Thermo Fisher	Cat# L10119
Cytofix/Cytoperm Kit	BD Bioscience	Cat# 554714
PE Annexin V Apoptosis Detection Kit with 7-AAD	Biolegend	640934
Alexa Fluor 594 Antibody Labeling Kit	ThermoFisher	A20185
Experimental Models: Cell Lines		
Vero cells	CSL Australia	N/A
Experimental Models: Organisms/Strains		
Mouse: C57BL/6J	The Jackson Laboratory	Stock# 000644; RRID: IMSR_JAX:000664
Mouse: B6.SJL-PtprcaPep3b/BoyJ (CD45.1)	The Jackson Laboratory	Cat# JAX:002014, RRID:IMSR_JAX:002014
Mouse: OBI x B6.129S7-*Rag1*^{tm1Mom}/J (OBI.RAG$^{-/-}$)	Dougan et al., 2012	N/A
Mouse: Ifnar2$^{-/-}$	N/A	N/A
Mouse: B6.129S2-*Ighm*^{tm1Cgn}/J (μMT$^{-/-}$)	The Jackson Laboratory	Cat# JAX:002288, RRID:IMSR_JAX:002288
Mouse: B6.129S4-*Ccr2*^{tm1Ifc}/J (CCR2$^{-/-}$)	The Jackson Laboratory	Cat# JAX:004999, RRID:IMSR_JAX:004999
Software and Algorithms		
Imaris version 9.2.1	https://imaris.oxinst.com/packages	RRID: SCR_007370

(*Continued on next page*)

Continued

REAGENT or RESOURCE	SOURCE	IDENTIFIER
FlowJo version 10 (Treestar inc)	https://www.flowjo.com	RRID: SCR_008520
Graphpad Prism 8	https://www.graphpad.com/scientific-software/prism/	RRID: SCR_002798
Adobe illustrator	https://www.adobe.com	RRID: SCR_010279
Other		
Nunc MaxiSorp flat-bottom	ThermoFisher	44-2404-21

RESOURCE AVAILABILITY

Lead Contact

Further information and requests for resources and reagents should be directed to Scott N. Mueller (smue@unimelb.edu.au)

Materials Availability

This study did not generate new unique reagents.

Data and Code Availability

This study did not generate/analyze datasets/codes

EXPERIMENTAL MODEL AND SUBJECT DETAILS

Mice

C57BL/6, B6.SJL-PtprcaPep3b/BoyJ (CD45.1), OBI x B6.129S7-*Rag1*^{tm1Mom}/J (OBI.RAG$^{-/-}$) (Dougan et al., 2012), *Ifnar2*$^{-/-}$, B6.129S2-*Ighm*^{tm1Cgn}/J (μMT$^{-/-}$) and B6.129S4-*Ccr2*^{tm1Ifc}/J (CCR2$^{-/-}$) mice were bred in the Department of Microbiology and Immunology. Animal experiments were approved by The University of Melbourne Animal Ethics Committee. Mice were maintained under specific pathogen free conditions and housed in individually ventilated cages containing cob bedding and environmental enrichment. All mice were sex and aged matched and used between 8-14 weeks old at the beginning of experiments.

Viruses

Herpes Simplex Virus-1 (HSV1) KOS strain, Lymphocytic choriomeningitis virus Armstrong strain and recombinant influenza virus X31 expressing the HSV glycoprotein-B-derived epitope gB$_{498–505}$.

METHOD DETAILS

Virus infections

Mice were infected subcutaneously (s.c.) in the footpad with either 5 × 10^4 plaque-forming units (PFU) of HSV-1 (KOS) or 2 × 10^4 PFU of LCMV (Armstrong). Mice were infected intranasally with 10^4 of the recombinant influenza virus X31 expressing the HSV glycoprotein-B-derived epitope gB$_{498–505}$ as described (Davies et al., 2017). For all infections, mice were anaesthetized with isoflurane vaporized in O_2. Unless stated otherwise mice were coinfected intraperitoneally with 2 × 10^5 PFU of LCMV Armstrong two days after footpad HSV infection. HSV-1 viral titers were determined in homogenized footpads by PFU assay as described (Jones et al., 2000).

Stromal cell isolation

LN were teased apart with forceps and incubated at 37°C in RPMI with 2mg/mL collagenase D, 0.8mg/mL Dispase and 100ug/mL DNase and 2% FBS for 25 minutes. Following a second round of digestion for 15 minutes, single cell suspensions were resuspended in FACS buffer (PBS 2% BSA 5mM EDTA) and filtered through 70 μM before antibody staining.

Lymphocyte isolation

For experiments where stromal cells were not analyzed, LN were mechanically dissociated through a a 70-μm nylon mesh in RPMI supplemented with 2% FBS.

Flow cytometry

Single cell suspensions were stained in FACS buffer containing CD16/32 Fc blocking antibody for 30min at 4°C. Live cells were discriminated with a fixable LIVE/DEAD Fixable Near-IR Dead Cell Stain Kit (Thermofischer). Annexin V staining was carried out

with Annexin V PE and 7AAD from Biolegend according to the manufacturer's instructions. Intracellular staining for KI67 and LCMV were performed using BD Cytofix/Cytoperm Fixation/Permeabilization Solution Kit according to the manufacturer's instructions. Purified LCMV antibody was conjugated to Alexa Fluor™ 594 with antibody labeling kit according to the manufacturer's instructions.

Endogenous HSV and LCMV-specific CD8 T cells were identified with H-2Kb-$gB_{498-505}$ and H-2Db-gp_{33-41} restricted tetramer staining respectively.

For metabolism analysis, cells were incubated with Mitotracker Deep Red FM, Bodipy FL C 16, CellROX orange reagent or 2-NBDG (all from ThermoFischer) in RPMI supplemented with 10% FCS for 30 minutes at 37°C except for 2-NBDG where glucose-free RPMI was used instead. Samples were acquired using FACSCantoII or FACSFortessa (both BD) and Flowjo software was used for analysis.

Immunomodulatory treatments

For $CD8^+$ T cell depletion, mice were injected i.p. twice with 100 μg of anti-CD8 antibody (clone 2.43), 24 hours apart. B cells were depleted with a single injection of 50 μg of anti-mouse CD20 antibody (clone 5D2, Genentech) prior HSV infection. To block lymphocyte egress, FTY720 (2-amino-2-(2-[4-octylphenyl]ethyl)-1,3-propanediol) was dissolved in 2% cyclodextrin in PBS and i.p. administered daily in mice at a dose of 1mg/kg from day 1 to day 7 post-HSV infection. Control mice were administered with 2% cyclodextrin only. To analyze the effect of systemic inflammation on local immune responses, HSV-infected mice were injected i.p. twice with either 50 μg Polyinosinic:polycytidylic acid high molecular weight (Poly(:IC)) or 5 μg of LPS, 24 hours apart. IFNAR *in vivo* blocking during coinfection was performed by injecting infected mice with 500 μg of anti-IFNAR-1 (clone MAR1-5A3) or isotype control antibody (clone MOPC-21, BioXcell) for two consecutive days and 250 μg on the third day. To block lymphocyte recruitment, mice were injected with 200 μg of blocking CD62-L, 1 day post-HSV infection and every two days until harvest. Immunization of mice was carried out by injecting 100 μg of OVA emulsified in CFA s.c.

Lymphocyte recruitment and cell egress analysis

C57BL/6-CD45.2 mice were infected s.c. with HSV and two days later injected i.v. with a mixture of 8 million total lymphocytes from pooled LN and spleen from C57BL/6-CD45.1 mice immediately prior to coinfection with LCMV. HSV draining and non-draining LN were analyzed 2 days post LCMV infection.

To analyze cell egress, mice were injected i.v. with a mixture of 8 million total lymphocytes from pooled LN and spleens from C57BL/6-CD45.1 mice. Two hours post cell transfer, mice were injected with 250 μg of blocking CD62-L antibody and LN were harvested 18h later. To define how many cells entered the LN, groups of mice were harvested two hours post cell transfer.

Generation of bone marrow chimeric mice

To generate IFNAR deficient B cell mice, C57BL/6-Ly5.1 recipient mice were lethally irradiated with two doses of 550 rads, 3 h apart, followed by reconstitution with a 80/20 mixture of 8×10^6 $\mu MT^{-/-}$ / WT or $\mu MT^{-/-}$ / *Ifnar2*$^{-/-}$ donor bone marrow cells and maintained in antibiotic water (neomycin and polymyxin B) for 4 weeks. To analyze the contribution of IFNAR signaling on hematopoietic and non-hematopoietic compartments, C57BL/6-Ly5.2 WT and *Ifnar2*−/− mice were irradiated and reconstituted with either 8×10^6 BM cells from WT or *Ifnar2*−/− donor mice. All recipients were used at least 8 weeks post-reconstitution.

Immunofluorescence and confocal microscopy

Lymph nodes were harvested and fixed in periodate-lysine-paraformaldehyde (PLP) fixative for 4 hours, incubated in 30% sucrose and embedded in OCT freezing media. LN were harvested and immediately embedded in OCT freezing media. Tissue sections were cut at 16 μm thickness with a cryostat (Leica CM3050S) and air-dried before being fixed in acetone for 5 min, dried, and then blocked for 30 min (Protein Block X0909, DAKO) at room temperature (RT). Sections were staining with primary antibodies for 1 hour at RT, washed in PBS and when required stained with secondary antibodies for 45 minutes at RT. Stained sections were mounted in ProLong Gold antifade reagent, and acquired on a LSM780 or LSM710 confocal microscope (Carl Zeiss) and images processed with Imaris.

Detection of HSV-1 IgG by ELISA

Nunc MaxiSorp round-bottom 96-well ELISA microtiter plates (Thermo Scientific) were coated overnight at 4°C with 10 μg/ml HSV-1 inactivated Vero cell extract. Unbound protein was washed away (PBS 0.05% Tween20) and serially diluted serum samples (PBS 0.5% BSA) were plated and incubated at RT for two hours. Bound mouse IgG Abs were detected using donkey anti-mouse IgG-HRP and visualized using o-Phenylenediamine. The OD readings were determined at 450/492 nm. Endpoint titers of anti-HSV-1 were calculated by using cut-off values defined as double the OD of non-infected serum control.

QUANTIFICATION AND STATISTICAL ANALYSIS

Quantification of cellularity

Cells were enumerated by adding SPHERO calibration particles to each sample before acquisition on flow cytometer.

Statistical analysis

Graphs and statistics were generated using Prism 8 (GraphPad). Samples were tested for normality and two groups were compared using two-tailed Mann-Whitney U-test or unpaired t test. Multiple groups were analyzed with one-way Anova followed by Tukey's post-test comparison or Kruskal-Wallis, based on Gaussian distribution. All graphs depict means ± SEM. Details of statistical analysis are indicated in the figure legends and include the statistical test used. ns, non-significant, *$p < 0.05$, **$p < 0.01$, *** $p < 0.001$, ****$p < 0.0001$.